Photovoltaic Microinverter using Single-stage Isolated High-frequency link Series Resonant Topology

Hariharan Krishnaswami, *Member, IEEE,*
Department of Electrical and Computer Engineering
The University of Texas at San Antonio
San Antonio, Texas, USA
E-mail: Hariharan.Krishnaswami@utsa.edu

***Abstract*— In this paper, PhotoVoltaic (PV) microinverter using a single-stage high-frequency ac link series resonant topology is proposed. The inverter has two active bridges, one at the front-end of PV module and the other at the output or utility side. The active bridges are interfaced through a series resonant tank and a high frequency transformer. A novel phase-shift modulation technique to regulate the current into utility is proposed. Steady-state analysis using sinusoidal approximation is presented to determine the magnitude of output current into utility. Soft-switching operation is ensured in all switches in the converter due to resonant nature of the circuit. The inverter has advantages of minimal power conversion stages, high-switching frequency operation and low switching losses and hence ideally suited for low power module integrated applications.**

I. Introduction

Microinverters, also known as AC modules or Module Integrated Converters (MIC), have been shown to have high energy yield in Photovoltaic (PV) generation system due to inverters for each individual PV module [1]. The plug and play feature of MIC is especially useful for low power residential applications. Several topologies of MIC have been proposed in literature [2], [3], [4], [5] which use high-frequency link based power conversion instead of traditional dc link based systems. In [2], a MIC is proposed which uses impedance-admittance conversion theory to supply current into the utility. In [3] a push-pull based dc-ac inverter with high frequency link is proposed. It has a matrix converter with four-quadrant switches at the secondary of the transformer. A flyback-based inverter is proposed in [4] with an unique power decoupling circuit at the output of the PV module. A full-bridge based high-frequency link inverter is proposed in [5] with lowered switching frequency of the matrix converter.

The principle of power conversion in most of these topologies is through an high frequency converter followed by a matrix converter. But leakage inductance of the transformer is a non-ideality and it creates high voltages across the output side converter switches, whenever current changes direction in one switching cycle. This causes severe voltage stress on the devices and reduces reliability. Having the inductance at the high frequency link and creating a high frequency current source which will then be rectified and fed to the utility as in [2], [6] can reduce the voltage stresses and also contribute to increased efficiency of power conversion.

In this paper a series resonant tank circuit is used at the high frequency link. The proposed converter consists of two active bridges, a high frequency transformer and a series resonant tank as shown in Fig. 1. The active bridges switch at constant switching frequency above resonant frequency. Phase-shift modulation technique between active bridges is proposed to control the current being fed to the utility as opposed to variable frequency and cycloconverter operation in [6]. The proposed principle of power conversion is similar to the dc-dc dual active bridge high power converter [7]. This principle is extended to dc-ac conversion for microinverter application with inductance replaced by a series resonant tank circuit in this paper. Four-quadrant full-bridge converter is used as the output side converter. In summary, the advantages of the proposed converter are,

- Reduced component count due to single conversion stage
- Reduced switching losses due to soft-switching operation in all the semiconductor switches
- Reduced size due to high switching frequency capability of the resonant nature of the circuit
- No adverse effect of voltage stresses on devices due to leakage inductance since it forms part of resonant circuit.

II. Proposed Phase-shift Modulation

The converter shown in Fig. 1 operates above resonant frequency f_r formed by the series resonant tank inductance L and capacitance C. The output of the solar module V_{in} is connected to the active bridge through a large capacitor which filters the current ripple at twice the line frequency. The active bridge at the output-side of the converter is connected to the load or the grid through a capacitive filter for filtering the switching frequency component of the output current. The input-side active bridge is modulated using the function $m_1(t)$ in (1) and the output side active bridge is modulated using $m_2(t)$ in (2). The function $sgn(.)$ is the signum function which denotes the sign of the signal. In the equations, ϕ is

This project was partially funded by CPSEnergy through its Strategic Research Alliance with The University of Texas at San Antonio.

978-1-4577-0541-0/11/$26.00 ©2011 IEEE

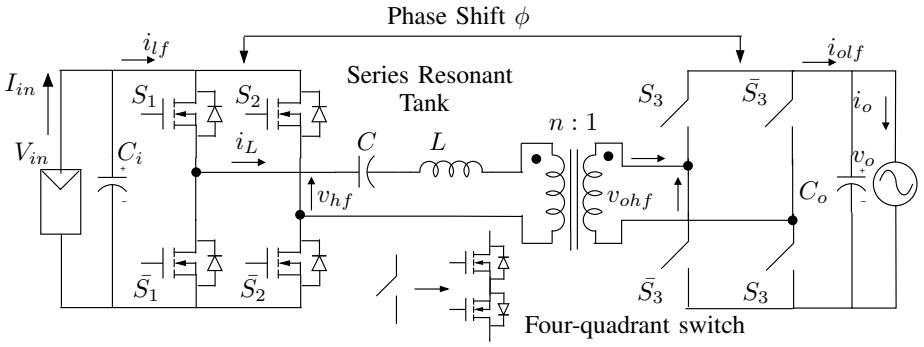

Fig. 1. Single-stage series-resonant microinverter

the phase-shift between the outputs of the active bridges v_{hf} and v_{ohf}, f_s is the switching frequency of the converter and f_o is the line frequency $60Hz$. The grid voltage is defined as $v_o(t) = \hat{V}_o \sin(\omega_o t)$.

$$m_1(t) = \frac{1}{2}\Big[sgn(\cos((\omega_s - \omega_o)t)) - sgn(\cos((\omega_s + \omega_o)t))\Big] \quad (1)$$

$$m_2(t) = sgn(\sin(\omega_s t - \phi)) \quad (2)$$

$$\text{where} \quad \omega_s = 2\pi f_s; \omega_o = 2\pi f_o \quad (3)$$

The switching signals to the Mosfets in Fig. 1 can be synthesized from (1) and (2). These switching signals are shown in Fig. 2. The left and the right leg switches of the input side active bridges are phase-shifted from each other by equal angles from a fixed reference and this phase-shift angle α as shown in Fig. 2 varies linearly starting from 0 to maximum value $\frac{T_s}{2}$, then to minimum value $-\frac{T_s}{2}$ and back to zero, where $T_s = \frac{1}{f_s}$. This variation is at a low frequency equal to the line frequency f_o. In Fig. 2, this fixed reference is at $\frac{T_s}{4}$. It is known that when a low frequency voltage waveform is amplitude modulated with a high frequency square wave $m_2(t)$ as in an electronic transformer, [8], the resultant Fourier spectrum has two fundamental frequencies $f_s - f_o$ and $f_s + f_o$. Since this voltage appears across the secondary of the transformer, it is necessary to produce a voltage waveform v_{hf} across the input of the series resonant tank with two fundamental frequencies. For this reason, the modulation function $m_1(t)$ takes the form given in (1).

Due to the filtering action of the series resonant tank, it can be assumed that all higher order harmonics are negligible in magnitude. Hence, the tank current is sinusoidal with two frequencies $f_s - f_o$ and $f_s + f_o$. Control of power flow is by phase-shifting the output-side active bridge with respect to the input-side active bridge and hence termed as phase-shift modulation. The principal of power flow is similar to the power flow between two buses in power systems. This phase-shift angle ϕ is given in (2). The switching signals of the Mosfets S_1, S_2 and S_3 are derived from the two modulation functions, as shown in Fig. 2. The switching signals can be generated using a double ramp carrier wave as given in [9]. This carrier wave aids in generating positive and negative phase-shifts α.

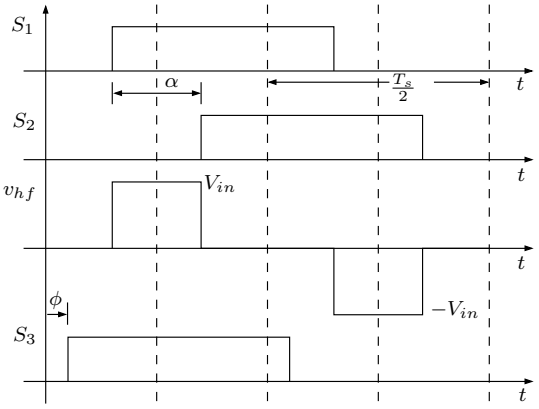

Fig. 2. Switching signals for the switches S_1, S_2 and S_3 shown for one switching cycle

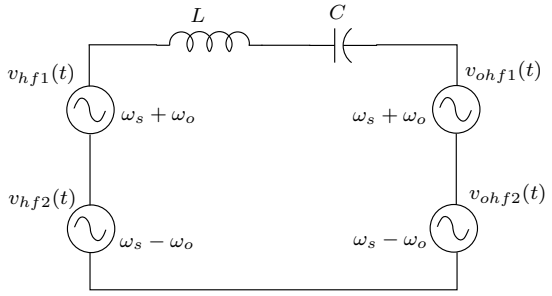

Fig. 3. Equivalent circuit for sinusoidal steady-state analysis

III. Steady-state analysis

Sinusoidal approximation is used in steady-state analysis since higher order harmonics are filtered by the resonant tank. Hence, only two frequencies are used in analysis, $f_s - f_o$ and $f_s + f_o$. The simplified equivalent circuit for analysis is shown in Fig. 3. The tank currents are calculated for each of the two frequencies using phasor analysis as given in (4) and (5).

$$\hat{I}_{L_1}\angle\theta_1 = \frac{\frac{2}{\pi}V_{in}\angle 0 - \frac{2}{\pi}\hat{V}_o\angle\phi}{j(\omega_s-\omega_o)L + \frac{1}{j(\omega_s-\omega_o)C}} \quad (4)$$

$$\hat{I}_{L_2}\angle\theta_2 = \frac{\frac{2}{\pi}V_{in}\angle 0 - \frac{2}{\pi}\hat{V}_o\angle\phi}{j(\omega_s+\omega_o)L + \frac{1}{j(\omega_s+\omega_o)C}} \quad (5)$$

The fundamental of v_{ohf} calculated from Fourier series leads to the constants $\frac{2}{\pi}$ in the equations. The inductor current is converted to a low frequency f_o by the output side bridge through the modulation function $m_2(t)$. The average current in one switching cycle T_s can be calculated by integrating the current between the limits ϕ and $\pi+\phi$. The integration for the inductor current with frequency $\omega_s-\omega_o$ is shown in (6). Similar integration applies for the inductor current with frequency $\omega_s+\omega_o$.

$$\bar{I}_{L_1} = \frac{1}{\pi}\int_{\phi}^{\pi+\phi} \hat{I}_{L_1}\sin((\omega_s-\omega_o)t-\theta_1)d(\omega_s t) \quad (6)$$

The following two assumptions are used since $f_s \gg f_o$:

- The average value of the output current remains constant in one switching cycle and
- The impedance of the resonant tank remains same for variations in frequency from $f_s - f_o$ to $f_s + f_o$ and the impedance at switching frequency is used for analysis.

With the application of the above two assumptions and simplifying the equations, the resultant average output current $\bar{i}_o(t)$ is given in (7). The output current is sinusoidal with the direction of the current indicated in Fig. 1. The current is in phase with utility voltage and hence power is fed back to the utility at unity power factor. The transformer turns ratio n is included in the equation.

$$\bar{i}_o(t) = \frac{8}{\pi^2}\frac{nV_{in}\sin\phi}{Z(F-\frac{1}{F})}\sin(\omega_o t) \quad (7)$$

$$\text{where } Z = \sqrt{\frac{L}{C}}\ ;\ F = \frac{\omega_s}{\omega_r}\ ;\ \omega_r = 2\pi f_r = \frac{1}{\sqrt{LC}} \quad (8)$$

The analysis equations are converted to per unit representation by choosing the output power as P_{base} and the line voltage rms as V_{base}. This conversion helps in designing the system for varied power and input voltage levels. The variable d termed as voltage conversion ratio is defined in (9). Dividing (7) by the base current, the resultant normalized output current is given in (10). In Section IV, a design procedure is discussed.

$$d = \frac{V_{in}}{nV_{o(rms)}\sqrt{2}} \quad (9)$$

$$\bar{i}_{o,pu}(t) = \frac{d\sin\phi}{Q(F-\frac{1}{F})}\sin(\omega_o t) \quad (10)$$

$$\text{where } Q = \frac{Z}{\frac{8}{\pi^2}n^2R_{base}}\ ;\ R_{base} = \frac{V_{base}^2}{P_{base}} \quad (11)$$

TABLE I
SERIES RESONANT DC-AC CONVERTER PARAMETERS

Converter Parameter	Value
Resonant Inductor L	$10.68\mu H$
Resonant Capacitor C	$0.3\mu F$
Input voltage V_{in}	$29.1V$
Line voltage rms $V_{o(rms)}$	$120V$
Maximum power output P_{base}	$225W$
Turns ratio n	0.17
Quality factor Q	4.0

IV. DESIGN

The design of the converter is based on the per unit equations in Section III. For the series resonant circuit, the quality factor is chosen as 4.0 or higher for validity of sinusoidal approximation. The ratio of switching frequency to resonant frequency is chosen as $F = 1.1$, to enable soft-switching operation. The voltage conversion ratio is chosen as $d = 1.0$ to enable wider range of soft-switching operation as in [7], [10]. With these chosen values, the value of phase-shift can be calculated from the required per unit current into the grid.

As an example, a $225W$ solar module from BP solar is chosen and the maximum power point (MPPT) mentioned in the datasheet $V_{max} = 29.1V$ and $I_{max} = 7.7A$ is used for simulation, although in real systems, MPPT can change based on sun's irradiance. MPPT can be implemented in this converter by appropriately varying the phase-shift angle ϕ. Since this converter is single-phase utility interactive, the grid voltage used in the simulation is $120V$ rms at a frequency of $60Hz$. The switching frequency f_s is chosen as $100kHz$. The converter parameters are calculated using (8) and (11). The values used in the converter simulation are summarized in Table I.

The converter can be represented using two state equations, with the inductor current and the capacitor voltage being the state variables. The input voltage V_{in} and the grid voltage $v_o(t)$ can be considered as ideal voltage sources. The state equations are given in (12-13).

$$\dot{i}_L = \frac{V_{in}}{L}m_1(t) - \frac{1}{L}v_C - \frac{n}{L}v_o(t)m_2(t) \quad (12)$$

$$\dot{v}_C = \frac{1}{C}i_L \quad (13)$$

These equations are simulated in Simulink and the ideal waveforms of the applied voltage across the tank v_{hf}, the transformer voltage v_{ohf} and the unfiltered output current i_{olf} are shown in Fig. 4 for one switching cycle T_s. In this figure, two instants are shown, which are the positive and negative peak of the grid voltage. The values used in this simulation is given in Table I.

V. SOFT-SWITCHING OPERATION

One of the advantages of operating the series resonant converter above resonant frequency is soft-switching. The

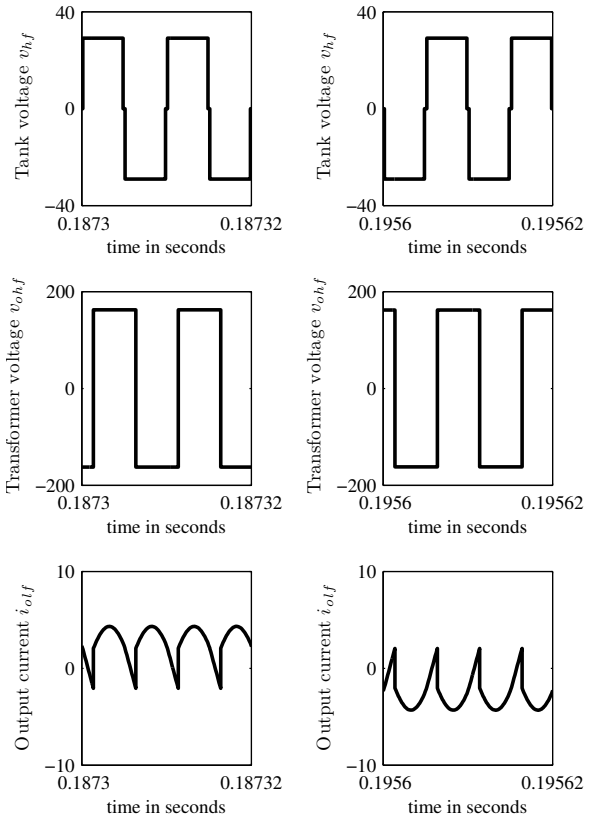

Fig. 4. Ideal waveforms of applied tank voltage v_{hf}, transformer voltage v_{ohf} and unfiltered output current i_{olf} for two switching cycles at two instants, positive and negative peak in line voltage

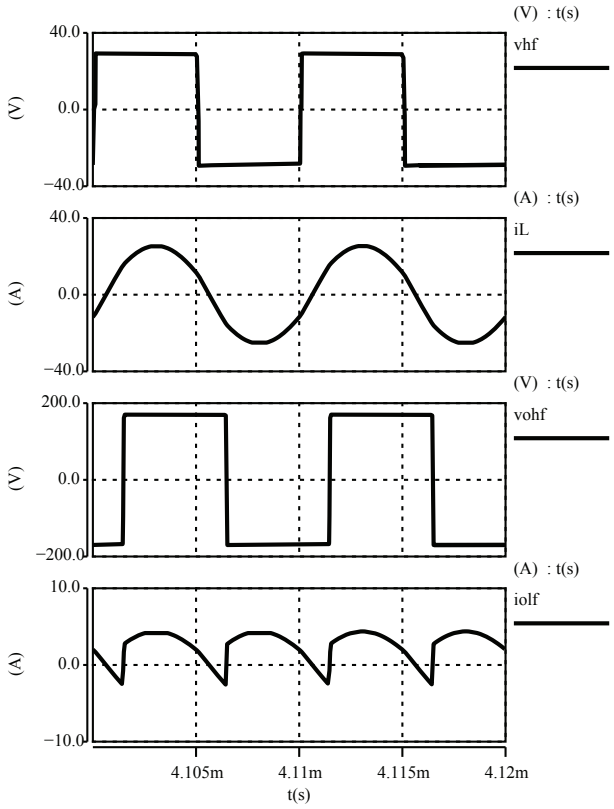

Fig. 5. Simulation results of tank current $i_L(t)$, applied tank voltage $v_{hf}(t)$, transformer voltage $v_{ohf}(t)$ and unfiltered output current $i_{olf}(t)$ shown for two switching cycles around the positive maximum of line voltage $v_o(t)$

tank current always lags the applied tank voltage and hence Zero Voltage Switching (ZVS) in all switches in input-side converter. But, the tank voltage is not a square-wave as it has zero voltage states, as shown in Fig. 2. Hence, for low values of α, one of the legs loses ZVS operation.

Based on the current direction shown in Fig. 1, the condition for soft-switching operation in the output-side active bridge is the transformer secondary current leading the voltage across the transformer. As long as the voltage conversion ratio is unity, soft-switching operation is possible in the output-side converter also. The active bridge at the output-side uses four-quadrant switches. In order to achieve soft-switching, one of the two Mosfets in a four-quadrant switch is always kept ON based on the polarity of the line voltage. This ensures that the other switch performs ZVS, based on the condition that the transformer secondary current leads v_{ohf}. Simulation results are given in the following section to prove soft-switching operation.

VI. Simulation results

In this section, the simulation results from Saber© are presented using the converter values summarized in Table I. Simulation results of the tank current in one switching cycle along with the applied tank voltage is shown in Fig. 5 for a phase-shift angle of $\alpha = 50^o$. The time instant during which the line voltage $v_o(t)$ is at its positive maximum is chosen for this plot. Due to the lagging nature of the current as observed from Fig. 5, soft-switching operation in the input-side bridge is ensured. The tank current leads the voltage across the transformer which ensures ZVS in output-side bridge. This is made possible by switching only one of the Mosfets in the four-quadrant switch shown in Fig. 1 according to polarity of line voltage and the other switch is ON continuously. The waveforms are repeated in Fig. 6 for the time instant at which the line voltage is at its minimum. It can be observed that soft-switching operation is ensured in this case also.

The filtered output current along with the line voltage is shown in Fig. 7. It is observed that line voltage and line current in the direction indicated in Fig. 1 are in phase and hence power is being fed to the utility. The analysis results match with the simulation results with an error of $< 5\%$ due to the sinusoidal approximation. The input current has a second harmonic component of the line frequency. The capacitor C_i at the input can be designed to filter this harmonic component. The tank current and its Fourier spectrum are shown in Fig. 8 which confirms the analysis assumption.

The converter efficiency is improved due to reduction in switching losses achieved by ZVS. Due to the use of two

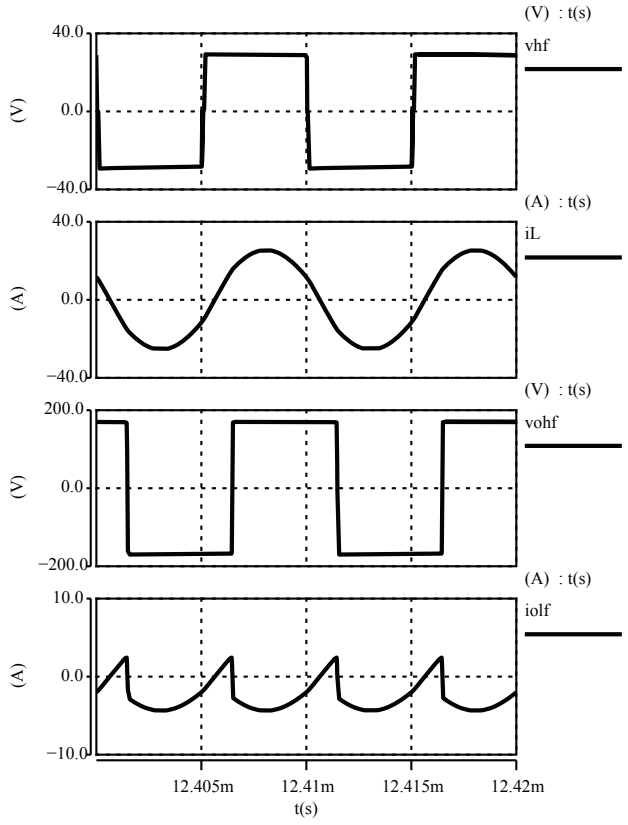

Fig. 6. Simulation results of tank current $i_L(t)$, applied tank voltage $v_{hf}(t)$, transformer voltage $v_{ohf}(t)$ and unfiltered output current $i_{olf}(t)$ shown for two switching cycles around the negative maximum of line voltage $v_o(t)$

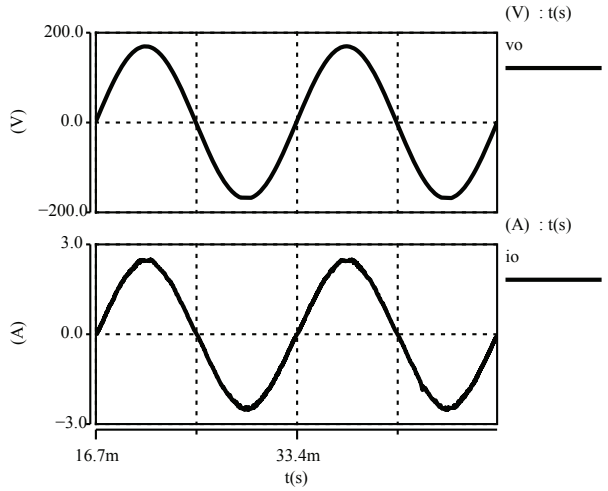

Fig. 7. Line voltage $v_o(t)$ and current $i_o(t)$ for two $60Hz$ cycles

semiconductor switches to realize a four-quadrant switch in the output-side converter, one of which is continuously ON based on grid voltage, the conduction losses can increase two-fold. But, since the switches are at the high voltage

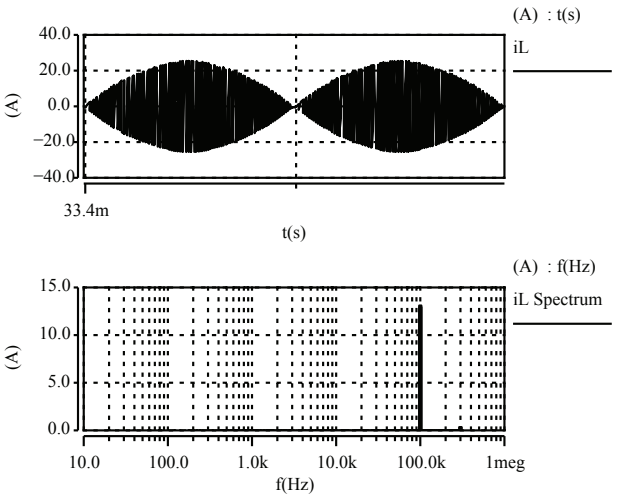

Fig. 8. Tank current $i_L(t)$ and its Fourier spectrum

side $< 200V$ and the currents are lower, it is possible to design the converter such that the effect of conduction losses on efficiency is minimal. The effect of increased cost of the converter due to addition of four-quadrant semiconductor switches in the output side converter is minimized by reduction in overall component count due to the use of single-stage power conversion as compared to the conventional two-stage dc-dc and dc-ac conversion.

VII. Conclusion

In this paper, a single-stage series resonant based photovoltaic microinverter is proposed. A novel phase-shift modulation technique to control the current into the grid is proposed along with steady-state analysis using sinusoidal approximation. Soft-switching operation is achieved in all the semiconductor switches. Simulation results are presented to verify the analysis. Experimental results under closed loop operation is part of further research in this project.

References

[1] Q. Li and P. Wolfs, "A review of the single phase photovoltaic module integrated converter topologies with three different dc link configurations," *Power Electronics, IEEE Transactions on*, vol. 23, no. 3, pp. 1320–1333, May 2008.

[2] S. Yatsuki, K. Wada, T. Shimizu, H. Takagi, and M. Ito, "A novel ac photovoltaic module system based on the impedance-admittance conversion theory," in *Power Electronics Specialists Conference, 2001. PESC. 2001 IEEE 32nd Annual*, vol. 4, 2001, pp. 2191–2196 vol. 4.

[3] K. de Souza, M. de Castro, and F. Antunes, "A dc/ac converter for single-phase grid-connected photovoltaic systems," in *IECON 02 [Industrial Electronics Society, IEEE 2002 28th Annual Conference of the]*, vol. 4, Nov. 2002, pp. 3268–3273 vol.4.

[4] T. Shimizu, K. Wada, and N. Nakamura, "Flyback-type single-phase utility interactive inverter with power pulsation decoupling on the dc input for an ac photovoltaic module system," *Power Electronics, IEEE Transactions on*, vol. 21, no. 5, pp. 1264–1272, Sept. 2006.

[5] S. Deng, H. Mao, J. Mazumdar, I. Batarseh, and K. Islam, "A new control scheme for high-frequency link inverter design," in *Applied Power Electronics Conference and Exposition, 2003. APEC '03. Eighteenth Annual IEEE*, vol. 1, Feb. 2003, pp. 512–517 vol.1.

[6] A. Trubitsyn, B. Pierquet, A. Hayman, G. Gamache, C. Sullivan, and D. Perreault, "High-efficiency inverter for photovoltaic applications," in *Energy Conversion Congress and Exposition (ECCE), 2010 IEEE*, 2010, pp. 2803 –2810.

[7] M. H. Kheraluwala, R. W. Gascoigne, D. M. Divan, and E. D. Baumann, "Performance characterization of a high-power dual active bridge dc-to-dc converter," *IEEE Trans. Ind. Appl.*, vol. 28, no. 6, pp. 1294–1300, Nov. 1992.

[8] M. Kang, P. Enjeti, and I. Pitel, "Analysis and design of electronic transformers for electric power distribution system," *Power Electronics, IEEE Transactions on*, vol. 14, no. 6, pp. 1133–1141, Nov 1999.

[9] H. Krishnaswami and V. Ramanarayanan, "Control of high-frequency ac link electronic transformer," *Electric Power Applications, IEE Proceedings -*, vol. 152, no. 3, pp. 509–516, May 2005.

[10] H. Krishnaswami and N. Mohan, "Three-port series-resonant dcdc converter to interface renewable energy sources with bidirectional load and energy storage ports," *Power Electronics, IEEE Transactions on*, vol. 24, no. 10, pp. 2289–2297, Oct. 2009.